Published on 12 February 2018. Downloaded by Freie Universitaet Berlin on 2/14/2020 9:41:55 AM.

Nanoscale

PAPER

View Article Online
View Journal | View Issue

Cite this: *Nanoscale*, 2018, **10**, 5358

Free charges *versus* excitons: photoluminescence investigation of InGaN/GaN multiple quantum well nanorods and their planar counterparts†

Weijian Chen, [a] Xiaoming Wen, *[b] Jianfeng Yang, [a] Michael Latzel,[c,d] Robert Patterson,[a] Shujuan Huang,[a] Santosh Shrestha, [a] Baohua Jia,[b] David J. Moss, [b] Silke Christiansen [c,e,f] and Gavin Conibeer*[a]

Received 11th October 2017, Accepted 11th February 2018

DOI: 10.1039/c7nr07567g

rsc.li/nanoscale

InGaN/GaN multiple quantum well (MQW) nanorods have demonstrated significantly improved optical and electronic properties compared to their planar counterparts. However, the exact nature of the processes whereby nanorod structures impact the optical properties of quantum wells is not well understood, even though a variety of mechanisms have been proposed. We performed nanoscale spatially resolved, steady-state, and time-resolved photoluminescence (PL) experiments confirming that photoexcited electrons and holes are strongly bound by Coulomb interactions (*i.e.*, excitons) in planar MQWs due to the large exciton binding energy in InGaN quantum wells. In contrast, free electron–hole recombination becomes the dominant mechanism in nanorods, which is ascribed to efficient exciton dissociation. The nanorod sidewall provides an effective pathway for exciton dissociation that significantly improves the optical performance of InGaN/GaN MQWs. We also confirm that surface treatment of nanorod sidewalls has an impact on exciton dissociation. Our results provide new insights into excitonic and charge carrier dynamics of quantum confined materials as well as the influence of surface states.

Introduction

After significant progress in the last decade,[1–5] InGaN/GaN multiple quantum wells (MQWs) are now being widely used for high-efficiency light-emitting diodes (LEDs). Furthermore, post-growth fabrication into nanorods has proved to be an effective method to boost the LED device efficiency[6–8] as compared to the as-grown thin film layers. Previously, researchers argued that these improvements were the result of a combination of in-plane strain relaxation, a decrease in the quantum-confined Stark effect (QCSE), light extraction efficiency enhancement and lateral carrier confinement.[6,9–11] However, detailed analyses of carrier dynamics are still unable to explain the change in luminescence properties of MQW nanorods over planar layers with respect to their carrier density dependence.[12–15] In particular, the impact of the significant increase of surface states in nanorods is not fully understood. A significant enhancement in the PL efficiency of nanorods is in contrast to the fact that enhanced non-radiative recombination – expected in nanorods due to surface damage – is actually detrimental to the radiative efficiency.[16–18] As we reported previously,[8] suitable surface treatment dramatically improves the performance of InGaN/GaN MQW nanorods. While it has been demonstrated that there is only a negligible strain change in the nanorods with such treatments,[8] an understanding of the detailed mechanisms of the performance improvement in nanorods is urgently required in order to further optimize InGaN/GaN MQW structures and performance.

There has been a significant debate in the community on the carrier recombination dynamics of InGaN quantum wells – whether it originates from free electron–hole[19] or excitonic recombination.[20,21] Given the large exciton binding energy in InGaN quantum wells due to a strong quantum confinement effect,[22] the presence of both free carriers and excitons should

[a]*Australian Centre for Advanced Photovoltaics, School of Photovoltaic and Renewable Energy Engineering, UNSW Sydney, Sydney 2052, Australia. E-mail: g.conibeer@unsw.edu.au*
[b]*Centre for Micro-Photonics, Swinburne University of Technology, Hawthorn 3122, Australia. E-mail: xwen@swin.edu.au*
[c]*Max Planck Institute for the Science of Light, Staudtstr. 2, 91058 Erlangen, Germany*
[d]*Institute of Optics, Information and Photonics, Friedrich-Alexander-Universität Erlangen-Nürnberg (FAU), Staudtstr. 7/B2, 91058 Erlangen, Germany*
[e]*Institute of Nanoarchitectures for Energy Conversion, Helmholtz-Zentrum Berlin für Materialien und Energie GmbH, Hahn-Meitner-Platz 1, 14109 Berlin, Germany*
[f]*Department of Physics, Freie Universität Berlin, Arnimallee 14, 14195 Berlin, Germany*

† Electronic supplementary information (ESI) available. See DOI: 10.1039/c7nr07567g

This journal is © The Royal Society of Chemistry 2018

Published on 12 February 2018. Downloaded by Freie Universitaet Berlin on 2/14/2020 9:41:55 AM.

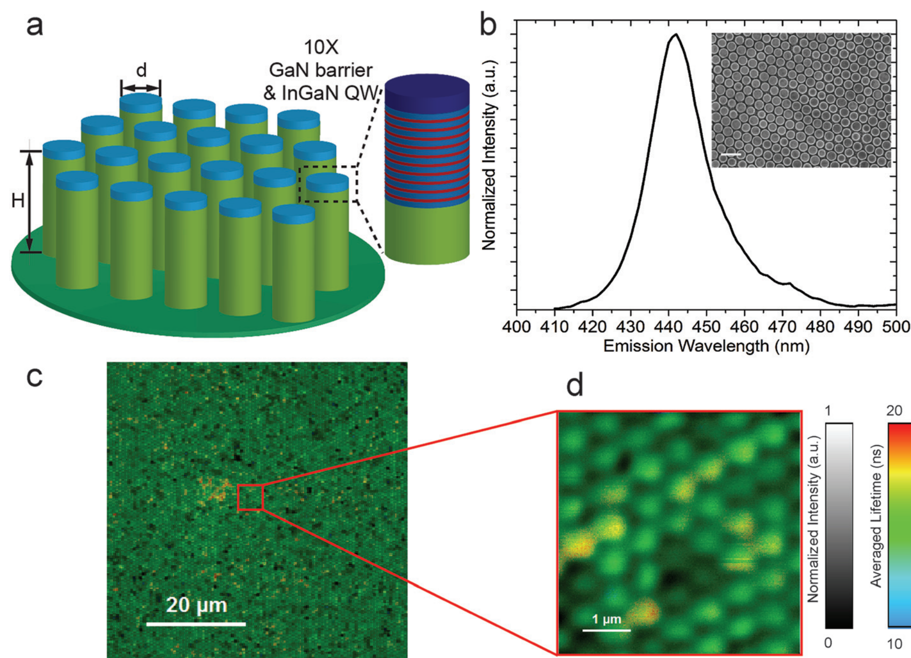

Fig. 1 (a) Schematic of the nanorods: H = 1.2 μm; d = 500 nm and 350 nm, for large and small nanorods, respectively; 10 stacks of InGaN/GaN MQWs are located at the top; (b) steady-state PL spectrum of the InGaN/GaN MQW small nanorods, the inset is the SEM image of the small nanorod array (the scale bar is 1 μm); (c) FLIM image of the as-etched large nanorods over a 60 × 60 μm^2 area and (d) a 5 × 5 μm^2 area indicated by the red rectangle in (c).

be considered in density dependent carrier dynamics studies, which has recently been suggested.[12,23,24] Even at room temperature, a rapid formation of excitons results in a significant exciton fraction in the total carrier population in InGaN quantum wells, as quantitatively calculated by Hangleiter *et al.*[24] Blancon *et al.* recently[25] proposed that the lower energy states at the layer edges/surface area of perovskite nanoplatelets could directly facilitate exciton dissociation.

To date, there is no study on exciton dissociation at the surface of InGaN/GaN MQW nanorods. Here, we study the density dependent recombination dynamics in InGaN/GaN MQW planar layers and nanorods by employing spatially resolved time integrated and time-resolved photoluminescence (TRPL). We find that exciton recombination is a dominant process in InGaN/GaN MQW planar layers, whereas free electron–hole recombination plays a dominant role in nanorods. The details of the photonic structure of the nanorod array have a negligible impact. We find that the surface states at the rod sidewall surfaces facilitate the dissociation of excitons in the InGaN/GaN MQWs.

Results and discussion

InGaN/GaN MQW planar layers were grown on a *c*-plane sapphire substrate by metalorganic vapor phase epitaxy (MOVPE).[26] Densely packed nanorods were then fabricated using a top-down etching method, as previously reported.[8] Detailed layer stacks are shown in Fig. S1 in the ESI.† Nanorods with two different as-etched diameters (500 nm and 350 nm) were fabricated (as shown in Fig. 1(a)), hereinafter referred to as large and small nanorods, respectively. The PL of the InGaN/GaN MQW nanorods with a diameter of 350 nm peaks at 442 nm, as shown in Fig. 1(b), displays a minor blueshift compared to planar layers (Fig. S4, ESI†) as a result of the reduced quantum confined Stark effect (QCSE) due to strain relaxation in the MQWs.[9] Fig. 1(c) and (d) display PL images of the large nanorods using fluorescence lifetime imaging microscopy (FLIM), which demonstrates the high quality of the nanorod PL uniformity by simultaneously mapping the PL intensity (brightness) and lifetime (color).[15] For a more intuitive assessment of the morphology and luminescence uniformity, the intensity and lifetime mapping are also separated into two images from Fig. 1(c) & (d), shown in section 2 of the ESI,† as well as a SEM and a cathodoluminescence (CL) mapping image.

We investigated the injected carrier density dependent PL response of the InGaN/GaN MQWs in MQW planar layer stacks as well as the large and small nanorods. The PL intensity of the nanorods is much stronger than that of the planar layers, as shown in Fig. 2(a)–(c). The PL enhancement in the nanorods has been attributed to various effects including strain relaxation,[9] excitation light in-coupling enhancement,[27,28] higher light extraction efficiency,[10] and lateral carrier confinement (see ESI section 4†). Fig. 2(d) shows the PL efficiency as a function of the injected carrier density. The relative PL efficiency is defined as $PL_{eff} = I_{em}/I_{ex}$, where I_{em} is the PL intensity and I_{ex} is the excitation power density.

Published on 12 February 2018. Downloaded by Freie Universitaet Berlin on 2/14/2020 9:41:55 AM.

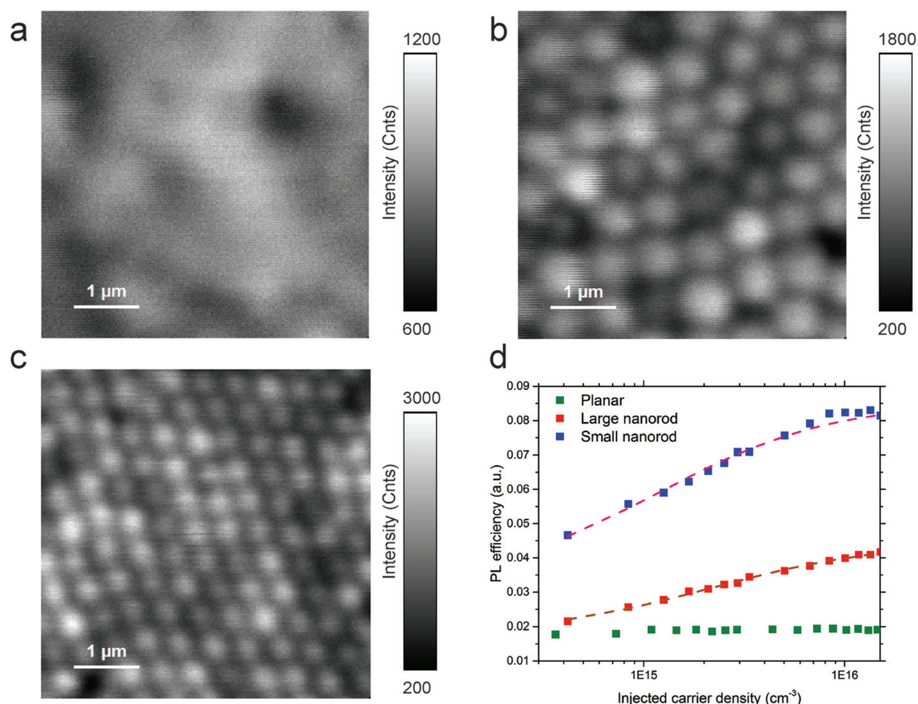

Fig. 2 PL intensity images of (a) planar layers, (b) large nanorods and (c) small nanorods over a 5 × 5 μm^2 area under the same injected carrier density; (d) PL efficiency as a function of the injected carrier density for the InGaN/GaN MQW planar layers and nanorods.

The injected carrier density of each excitation power is calculated accordingly,[29] where quasi-planar absorption in nanorods is applied, as discussed in detail in ESI section 5.†

The planar layers and nanorods exhibit distinctly different dependences of PL efficiency on the injected carrier density, as shown in Fig. 2(d). The PL efficiency of the planar layers is constant, independent of the increase in injected carrier density, whereas the nanorods exhibit a PL efficiency that increases dramatically with the injected carrier density, suggesting different recombination mechanisms for the two cases. The increasing PL efficiency with the injected carrier density observed from the nanorods is a signature of systems dominated by free electron–hole recombination, while the relatively flat PL efficiency is typical in systems dominated by exciton recombination.[30–33] Since the nanorods are fabricated from the same InGaN/GaN MQW planar layers, the only difference is the sidewall surface of the nanorods (as discussed below, the impact of the nanorod photonic structure can be excluded). It is reasonable to attribute the difference in PL behaviour between the MQW planar layers and nanorods to surface-related factors, such as surface defects of the nanorods, in the event that there is little etching damage on the surface in the planar layers.

The carrier density dependence of the steady-state PL response of the InGaN MQWs is quantitatively described using a carrier dynamics model comprised of excitons and free electron–holes.[34] Below the Mott density, the proportion of exciton population in the total carrier density is independent of the injected density at room temperature.[12] A modified rate equation is applied to describe the recombination dynamics in such a system, which includes free electron–hole[12] and exciton[35] recombination. In this model we focus on the low injection regime, in which the dynamic processes only include Shockley–Read–Hall (SRH) and free electron–hole and/or exciton radiative recombination, since the impact of Auger recombination is negligible within a relatively low range of the injected carrier densities.[12] Under steady state conditions, the PL efficiency is:

$$\mathrm{PL}_{\mathrm{eff}}(N) = \beta \frac{B'_{\mathrm{x}}N + B'_{\mathrm{eh}}N^2}{A'N/\eta + B'_{\mathrm{x}}N + B'_{\mathrm{eh}}N^2} \qquad (1)$$

where A', B'_{eh} and B'_{x} stand for the generalized coefficients of SRH recombination, electron–hole and exciton radiative recombination to the total carrier concentration N; β is a constant of proportionality and η is an output coupling coefficient that fits the experimental detection. A detailed discussion of the limitations of our method can be found in section 6 of the ESI.†

In an exciton dominated system, where $B'_{\mathrm{eh}}N^2 \ll B'_{\mathrm{x}}N$, eqn (1) is simplified into $\mathrm{PL}_{\mathrm{eff}}(N) = \beta B'_{\mathrm{x}}/(A'/\eta + B'_{\mathrm{x}})$, which is independent of the injected carrier density. The PL efficiency of the planar layers is therefore dominated by exciton recombination since it is independent of the injected carrier density (Fig. 2(d)). The PL efficiency of the nanorods, on the other hand, increases with an increase in injected carrier density. By fitting the nanorod PL efficiency using eqn (1), shown as the dashed lines in Fig. 2(d), the ratio between the radiative recom-

 This journal is © The Royal Society of Chemistry 2018

Published on 12 February 2018. Downloaded by Freie Universitaet Berlin on 2/14/2020 9:41:55 AM.

bination rates of electron–holes and excitons, $B'_{eh}N^2/(B'_xN)$, is revealed. This recombination rate ratio is carrier density dependent, which originates from the fact that free electron–hole recombination is proportional to the square of the carrier concentration ($B'_{eh}N^2$).

For convenience, in order to compare different samples, we define the recombination rate ratio at a carrier concentration of $N_m = 10^{16}$ cm^{-3} as a benchmark indicator of the relative contribution of free electron–hole recombination *versus* exciton recombination to the PL intensity. The recombination rate ratios, $B'_{eh}N_m^2/(B'_xN_m)$, are 12.4 and 13.6, for the large and small nanorods, respectively. As a comparison, this ratio for the planar layers is close to zero, confirming that exciton recombination is dominant. This observation clearly indicates that free electron–hole recombination plays an important role in nanorods, and increases as the rod diameters decrease.

We measured the carrier density dependent time-resolved PL for all three samples. Fig. 3(a) presents the PL decay traces of the planar layers and small nanorods for the same range of the injected carrier density. We see that the planar layers exhibit a weak density dependent PL decay, whereas the decay of the nanorod PL becomes significantly slower with the increase in injected carrier density. For a direct comparison of the power dependent TRPL, effective lifetimes τ_{eff} are extracted by exponential fitting of the corresponding TRPL decay traces: $I(t) = \sum_i A_i \cdot \exp(-t/\tau_i)$, where A_i stands for the amplitude and τ_i is the lifetimes of the respective decay channels. Here the PL decay traces could be well fit by a bi-exponential function. For a direct comparison among the TRPL decays of all samples, one can define the effective lifetime as $\tau_e = \sum_i (A_i\tau_i)/\sum_i (A_i)$.[36] The effective lifetimes *versus* the injected carrier density are shown in Fig. 3(b). Overall, it is evident that the effective lifetimes of the nanorods are generally much shorter than those of the planar layers. Faster PL decay rates in nanorods have been ascribed to the enhancement of both non-radiative and radiative recombination after rod etching, because of the larger number of surface defects,[8] as well as strain relaxation,[9] respectively. However, these mechanisms cannot explain the dramatic difference between the planar layers and nanorods in terms of their dependence of TRPL lifetimes on the injected carrier density. The effective PL lifetime of the planar layers only increases slightly with the increase in injected carrier density. The exciton radiative recombination is a monomolecular recombination process,[37] such that the PL decay is weakly dependent on the carrier density in the planar layers, where excitons dominate. In contrast, in the nanorods the lifetime increases significantly with the increase in injected carrier density, and this is even more evident for the small nanorods. The electron–hole radiative recombination is a bimolecular process and thus depends significantly on the carrier density. At first glance, this seems counterintuitive as one might argue that the PL decay lifetime should decrease with the increase in carrier density, if solely considering a bimolecular process. It should be noted that the PL decay is determined by a competition between non-radiative and radiative recombination processes. The dependence of lifetime on the carrier density not only depends on the electron–hole recombination rate, but also on the defect density, as discussed by Wen *et al.*[38]

Our measurements of the dependence of lifetimes on the injected carrier density consistently indicate that free electron–hole radiative recombination is a dominant process over exciton radiative recombination in the nanorods.

Our observations indicate that after etching the planar layers into nanorods, an effective pathway emerges to dissociate excitons into free carriers. With a larger portion of free electrons and holes in the nanorods, bimolecular radiative recombination plays a more important role than in the planar quantum wells. A stronger carrier density dependence is therefore observed in the nanorods than the planar quantum wells. Exciton dissociation is essentially governed by the Coulomb attraction between electrons and holes, and so intuitively one could ascribe exciton dissociation observed in the nanorods to a decrease in the exciton binding energy in the InGaN quantum wells after rod etching. It has been demonstrated that an increase in quantum confinement results in an increase in the binding energy.[39] However, there is no major change of the exciton binding energy due to quantum confine-

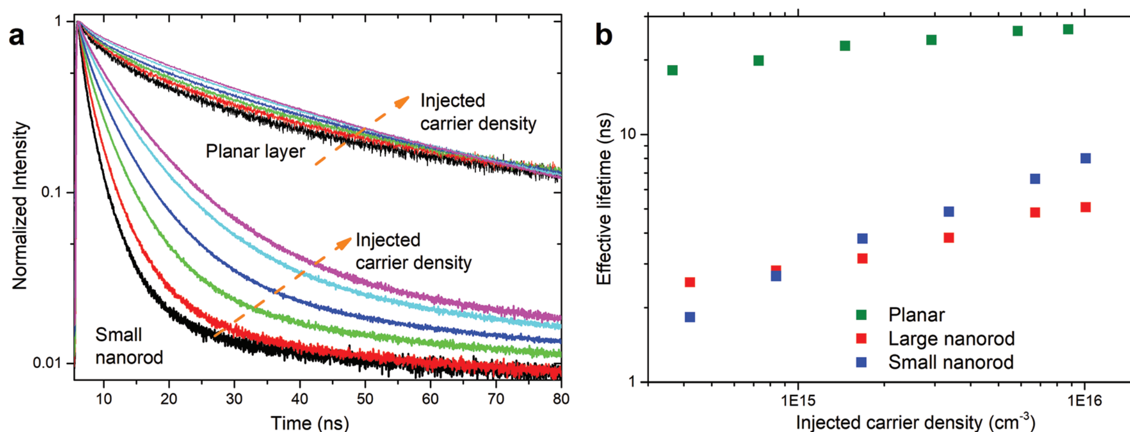

Fig. 3 (a) PL decay traces and (b) effective lifetimes as a function of carrier density for InGaN/GaN MQW planar layers and as-etched nanorods.

Published on 12 February 2018. Downloaded by Freie Universitaet Berlin on 2/14/2020 9:41:55 AM.

ment change, given that all three samples have the same quantum well structure and the diameters of the nanorods are much larger than the Bohr radius.[40] The exciton binding energy may change in the nanorods due to changes in strain. As studied in our earlier publications,[8,9] compressive strain states are completely relaxed in the GaN layers and partially relaxed in the InGaN quantum wells in the nanorods. This strain relaxation leads to a better spatial overlap between electron and hole wavefunctions (often referred to as oscillator strength), due to the reduced QCSE,[41] which also induces the blueshift in the PL peak of the MQWs in the nanorods (Fig. S4, ESI†). It is widely agreed that better spatial overlap between electron and hole wavefunctions leads to an increase in exciton binding energy,[42,43] although in our case this appears to be minor, since the increase of exciton binding energy counters the exciton dissociation in the nanorods. Therefore, the impact of any change in exciton binding energy in the nanorods is negligible.

Since the diameters and spacing of the nanorods are comparable to the excitation and emission optical wavelengths, in principle the impact of the overall photonic structure should be taken into account.[44,45] We performed PL measurements on sparse nanorods with different relative positions in nanorod clusters and confirmed that any details of the overall structure of the nanorod array (*e.g.*, the periodic hexagonal structure used here) have a negligible impact on the PL carrier density dependence. Three types of sparse nanorods have been studied here, namely the center rod, the edge rods of a nanorod cluster, and fully stand-alone rods, as shown in Fig. S7 (ESI).† We observed single point excitation in which the laser only excited a single rod (Fig. S7†), in comparison with the scanning mode in which the laser beam scanned from rod to rod in a large area (Fig. 1(d)). The sparse nanorods and the nanorod array had very similar PL behaviour and so the impact of the photonic structure can be excluded.

In this case, the sidewall surface of the nanorods, where the MQWs are exposed, could play a significant role. Given that the rod diameters are comparable to the diffusion length in InGaN quantum wells,[46,47] the nanorod sidewalls may facilitate exciton dissociation. With incident light excitation, the excitons effectively form in the InGaN MQW nanorods as the binding energy is significantly larger than the thermal energy.[22] These excitons can diffuse and arrive at the sidewall surface of the nanorods. It has been reported that excitons effectively dissociate at the various heterogeneous interfaces, such as organic semiconductors and perovskites.[25,48–52] It is expected that the excitons will more easily diffuse to the sidewalls in smaller nanorods, and will therefore result in more effective exciton dissociation and a higher proportion of free electrons and holes, which is consistent with our experimental observation.

Since the effect of the nanorods on the PL enhancement is to laterally confine the photogenerated carriers compared to the planar layers, it is expected that the electron–hole oscillator strength will be significantly enhanced in the nanorods. The radiative recombination rate in the nanorods is much larger than the planar layers. Therefore, the enhancement of radiative recombination is stronger than non-radiative recombination, even though surface defect densities are higher than the planar layers. We also infer that with further surface passivation the PL decay lifetime decreases due to decreased defect trapping, and as a consequence, the PL efficiency will further increase.

It is an unresolved problem as to why excitons can efficiently dissociate into free electrons and holes at the sidewalls – the driving force for this dissociation is still unknown, although some mechanisms have been proposed. For example, it has been shown that delocalization of charge carriers can help them overcome the Coulomb potential barrier in organic semiconductors.[53,54] In perovskite nanoplatelets,[25] on the other hand, the lower energy edge states have been proposed to facilitate exciton dissociation. Given that sidewall surfaces facilitate exciton dissociation, it is also anticipated that surface treatment would change the exciton/free electron–hole dynamics in the nanorods. The nanorod sidewall surfaces were treated with KOH solution wet etching (hereinafter referred to as "KOH-etched"), and then coated with an Al_2O_3 thin layer using atomic layer deposition (hereinafter referred to as "Al_2O_3-coated"). As reported previously,[8] after KOH etching, the nanorod sidewalls are *m*-plane facets with clear kinks and vertical edges, whereas these kinks and edges are less prominent after the coating of Al_2O_3 layers.

We studied the injected carrier density dependent PL of the InGaN/GaN MQW nanorods after surface treatment (Fig. 4). Compared to the fast PL decay in the as-etched nanorods, the PL decay is significantly slower in both KOH-etched and Al_2O_3-coated nanorods (Fig. 4(a)), and the increase of the PL lifetime with the increase in injected carrier density is more pronounced (Fig. 4(b)). Meanwhile, the PL efficiency increases in both surface treated nanorods. The surface trap state densities in these nanorods are calculated using the model developed by Xing *et al.*,[55] as described in section 8 of the ESI† and the results are presented in Table 1. The enhancement of the nanorod PL performance is associated with a decrease in the surface defect density.

The surface treatments change the injected carrier density dependence of the PL efficiency, which is well fit by a modified rate equation model described above as shown in Fig. 4(c). In such surface-treated nanorods, the lower defect density results in a higher carrier density in the nanorods with the same injected density. The recombination rate ratio changes with each surface treatment: the recombination rate ratios, $B'_{eh}N_m^2/(B'_xN_m)$, of the KOH-etched samples (185) and the Al_2O_3-coated sample (45.6), are much larger than that of the as-etched sample (13.6). This suggests that the separated free electrons and holes are strongly trapped by surface states. In surface treated nanorods, saturation of PL efficiency was observed at high injected carrier densities, most likely due to an increase in Auger recombination that is not included in this low carrier density model. Surface treatment significantly decreases the surface trapping density and thus significantly increases the proportion of free carriers. Surface treatment evidently increases the PL effective lifetime and efficiency by decreasing the density

This journal is © The Royal Society of Chemistry 2018

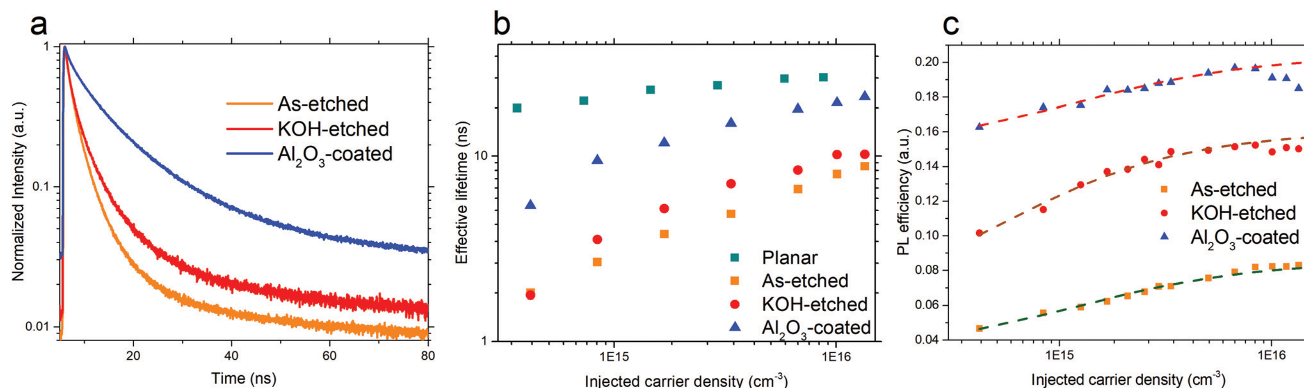

Fig. 4 (a) PL decay traces at low injected carrier density (10^{15} cm^{-3}), (b) effective lifetime & (c) PL efficiency as a function of the injected carrier density in the InGaN/GaN MQW small nanorods with/without rod surface treatment.

Published on 12 February 2018. Downloaded by Freie Universitaet Berlin on 2/14/2020 9:41:55 AM.

Table 1 Defect density of InGaN/GaN MQWs

Planar layers defect density (unit: 10^{14} cm^{-3})	Surface defect density of small nanorods (unit: 10^{14} cm^{-3})		
	As-etched	KOH-etched	Al_2O_3-coated
0.27	3.98	1.41	0.52

of defect trapping. This result supports the previous discussion that surface states at nanorod sidewalls strongly impact exciton dissociation in the InGaN/GaN MQW nanorods.

Conclusions

We have investigated steady state and time-resolved PL as a function of injected carrier density in InGaN/GaN MQW planar layers and nanorods. The planar layers exhibit exciton dominant behaviour while free electron–hole recombination dominates in the nanorods. This is attributed to the effective exciton dissociation that occurs at the nanorod sidewall surface. With further surface passivation, the PL efficiency in the nanorods is significantly increased and the PL lifetime increases, which is attributed to the decreased surface trapping density. These findings reveal the impact of surface states on carrier recombination dynamics in InGaN/GaN nanorods and will help pave the way for high-efficiency optoelectronic devices based on InGaN/GaN multiple quantum wells.

Conflicts of interest

There are no conflicts to declare.

Author contributions

X. Wen designed the experimental project and initiated the concept; W. Chen analyzed experimental results and wrote the manuscript with assistance from X. Wen, J. Yang and D. Moss; M. Latzel fabricated the samples. The manuscript was written through contributions of all authors. All authors have given approval to the final version of the manuscript.

Acknowledgements

This work is supported by the Australian Government through the Australian Renewable Energy Agency (ARENA), the European Union Seventh Framework Programme [FP7/2007–2013] under grant agreement number 280566, and the German Research Foundation (DFG) within the project "Dynamics and Interactions of Semiconductor Nanowires for Optoelectronics (FOR 1616)". The authors acknowledge DFG for financial support through the Cluster of Excellence Engineering of Advanced Materials at the University of Erlangen-Nürnberg, the Deutscher Akademischer Austauschdienst (DAAD) for an exchange scholarship and China Scholarship Council for life stipend. This work is also supported by the Australian Research Council Discovery Projects Program (DP150104327).

References

1 H. Masui, S. Nakamura, S. P. DenBaars and U. K. Mishra, *IEEE Trans. Electron Devices*, 2010, **57**, 88–100.
2 S. Pimputkar, J. S. Speck, S. P. DenBaars and S. Nakamura, *Nat. Photonics*, 2009, **3**, 180–182.
3 W. Guo, M. Zhang, A. Banerjee and P. Bhattacharya, *Nano Lett.*, 2010, **10**, 3356–3359.
4 H. M. Kim, Y. H. Cho, H. Lee, S. I. I. Kim, S. R. Ryu, D. Y. Kim, T. W. Kang and K. S. Chung, *Nano Lett.*, 2004, **4**, 1059–1062.
5 Y. J. Lee, S. Y. Lin, C. H. Chiu, T. C. Lu, H. C. Kuo, S. C. Wang, S. Chhajed, J. K. Kim and E. F. Schubert, *Appl. Phys. Lett.*, 2009, **94**, 92–95.
6 B. Liu, R. Smith, J. Bai, Y. Gong and T. Wang, *Appl. Phys. Lett.*, 2013, **103**, 101108.
7 J. Bai, Q. Wang and T. Wang, *J. Appl. Phys.*, 2012, **111**, 113103.

Published on 12 February 2018. Downloaded by Freie Universitaet Berlin on 2/14/2020 9:41:55 AM.

8 M. Latzel, P. Büttner, G. Sarau, K. Höflich, M. Heilmann, W. Chen, X. Wen, G. Conibeer and S. H. Christiansen, *Nanotechnology*, 2017, **28**, 55201.
9 G. Sarau, M. Heilmann, M. Latzel and S. Christiansen, *Nanoscale*, 2014, **6**, 11953–11962.
10 S. W. Schmitt, G. Sarau and S. Christiansen, *Sci. Rep.*, 2015, **5**, 17089.
11 M. L. Kuo, Y. S. Kim, M. L. Hsieh and S. Y. Lin, *Nano Lett.*, 2011, **11**, 476–481.
12 W. Liu, R. Butté, A. Dussaigne, N. Grandjean, B. Deveaud and G. Jacopin, *Phys. Rev. B: Condens. Matter Mater. Phys.*, 2016, **94**, 195411.
13 N. Shimosako, Y. Inose, H. Satoh, K. Kinjo, T. Nakaoka, T. Oto, K. Kishino and K. Ema, *J. Appl. Phys.*, 2015, **118**, 175702.
14 C. Shi, C. Zhang, F. Yang, M. J. Park, J. S. Kwak, S. Jung, Y.-H. Choi, X. Wang and M. Xiao, *Opt. Express*, 2014, **22**, A790–A799.
15 W. Chen, X. Wen, M. Latzel, M. Heilmann, J. Yang, X. Dai, S. Huang, S. Shrestha, R. Patterson, S. Christiansen and G. Conibeer, *ACS Appl. Mater. Interfaces*, 2016, **8**, 31887–31893.
16 P. A. Alekseev, M. S. Dunaevskiy, V. P. Ulin, T. V. Lvova, D. O. Filatov, A. V. Nezhdanov, A. I. Mashin and V. L. Berkovits, *Nano Lett.*, 2015, **15**, 63–68.
17 C. Zhao, T. K. Ng, A. Prabaswara, M. Conroy, S. Jahangir, T. Frost, J. O'Connell, J. D. Holmes, P. J. Parbrook, P. Bhattacharya and B. S. Ooi, *Nanoscale*, 2015, **7**, 16658–16665.
18 M. Boroditsky, I. Gontijo, M. Jackson, R. Vrijen, E. Yablonovitch, T. Krauss, C.-C. Cheng, A. Scherer, R. Bhat and M. Krames, *J. Appl. Phys.*, 2000, **87**, 3497.
19 Y. Xing, L. Wang, D. Yang, Z. Wang, Z. Hao, C. Sun, B. Xiong, Y. Luo, Y. Han, J. Wang and H. Li, *Sci. Rep.*, 2017, **7**, 45082.
20 Y.-C. Pu, M. G. Kibria, Z. Mi and J. Z. Zhang, *J. Phys. Chem. Lett.*, 2015, **6**, 2649–2656.
21 S. Boubanga-Tombet, J. B. Wright, P. Lu, M. R. C. Williams, C. Li, G. T. Wang and R. P. Prasankumar, *ACS Photonics*, 2016, **3**, 2237–2242.
22 S. Khatsevich and D. H. Rich, *J. Phys.: Condens. Matter*, 2008, **20**, 215223.
23 M. Shahmohammadi, G. Jacopin, G. Rossbach, J. Levrat, E. Feltin, J.-F. Carlin, J.-D. Ganière, R. Butté, N. Grandjean and B. Deveaud, *Nat. Commun.*, 2014, **5**, 5251.
24 A. Hangleiter, Z. Jin, M. Gerhard, D. Kalincev, T. Langer, H. Bremers, U. Rossow, M. Koch, M. Bonn and D. Turchinovich, *Phys. Rev. B: Condens. Matter Mater. Phys.*, 2015, **92**, 241305.
25 J.-C. Blancon, H. Tsai, W. Nie, C. C. Stoumpos, L. Pedesseau, C. Katan, M. Kepenekian, C. M. M. Soe, K. Appavoo, M. Y. Sfeir, S. Tretiak, P. M. Ajayan, M. G. Kanatzidis, J. Even, J. J. Crochet and A. D. Mohite, *Science.*, 2017, **355**, 1288–1292.
26 S. Meuret, T. Coenen, H. Zeijlemaker, M. Latzel, S. Christiansen, S. Conesa-Boj and A. Polman, *Phys. Rev. B: Condens. Matter Mater. Phys.*, 2017, **96**, 35308.
27 J. Zhu, Z. Yu, G. F. Burkhard, C.-M. Hsu, S. T. Connor, Y. Xu, Q. Wang, M. McGehee, S. Fan and Y. Cui, *Nano Lett.*, 2009, **9**, 279–282.
28 R. Jayaprakash, D. Ajagunna, S. Germanis, M. Androulidaki, K. Tsagaraki, A. Georgakilas and N. T. Pelekanos, *Opt. Express*, 2014, **22**, 19555.
29 Y. J. Lee, C. H. Chiu, C. C. Ke, P. C. Lin, T. C. Lu, H. C. Kuo and S. C. Wang, *IEEE J. Sel. Top. Quantum Electron.*, 2009, **15**, 1137–1143.
30 F. Vietmeyer, P. A. Frantsuzov, B. Janko and M. Kuno, *Phys. Rev. B: Condens. Matter Mater. Phys.*, 2011, **83**, 115319.
31 S. Draguta, S. Thakur, Y. V. Morozov, Y. Wang, J. S. Manser, P. V. Kamat and M. Kuno, *J. Phys. Chem. Lett.*, 2016, **7**, 715–721.
32 D. Ma, X. Rong, X. Zheng, W. Wang, P. Wang, T. Schulz, M. Albrecht, S. Metzner, M. Müller, O. August, F. Bertram, J. Christen, P. Jin, M. Li, J. Zhang, X. Yang, F. Xu, Z. Qin, W. Ge, B. Shen and X. Wang, *Sci. Rep.*, 2017, **7**, 46420.
33 C. He, Z. Qin, F. Xu, M. Hou, S. Zhang, L. Zhang, X. Wang, W. Ge and B. Shen, *Sci. Rep.*, 2015, **5**, 13046.
34 R. Huber, F. Tauser, A. Brodschelm, M. Bichler, G. Abstreiter and A. Leitenstorfer, *Nature*, 2001, **414**, 286–289.
35 S. Nakamura and S. F. Chichibu, *Introduction to nitride semiconductor blue lasers and light emitting diodes*, CRC Press, 2000.
36 X. Wen, P. Yu, Y.-R. Toh, Y.-C. Lee, K.-Y. Huang, S. Huang, S. Shrestha, G. Conibeer and J. Tang, *J. Mater. Chem. C*, 2014, **2**, 3826–3834.
37 J.-C. Blancon, W. Nie, A. J. Neukirch, G. Gupta, S. Tretiak, L. Cognet, A. D. Mohite and J. J. Crochet, *Adv. Funct. Mater.*, 2016, **26**, 4283–4292.
38 X. Wen, Y. Feng, S. Huang, F. Huang, Y.-B. Cheng, M. Green and A. Ho-Baillie, *J. Mater. Chem. C*, 2015, **4**, 793–800.
39 T. Someya, H. Akiyama and H. Sakaki, *Phys. Rev. Lett.*, 1996, **76**, 2965–2968.
40 P. Ramvall, S. Tanaka, S. Nomura, P. Riblet and Y. Aoyagi, *Appl. Phys. Lett.*, 1998, **73**, 1104–1106.
41 N. Susa, *IEEE J. Quantum Electron.*, 1996, **32**, 1760–1766.
42 S. de-Leon and B. Laikhtman, *Phys. Rev. B: Condens. Matter Mater. Phys.*, 2000, **61**, 2874–2887.
43 G. Bastard, E. E. Mendez, L. L. Chang and L. Esaki, *Phys. Rev. B: Condens. Matter Mater. Phys.*, 1982, **26**, 1974–1979.
44 A. A. Erchak, D. J. Ripin, S. Fan, P. Rakich, J. D. Joannopoulos, E. P. Ippen, G. S. Petrich and L. A. Kolodziejski, *Appl. Phys. Lett.*, 2001, **78**, 563–565.
45 D. Englund, D. Fattal, E. Waks, G. Solomon, B. Zhang, T. Nakaoka, Y. Arakawa, Y. Yamamoto and J. Vučković, *Phys. Rev. Lett.*, 2005, **95**, 13904.
46 Y. T. Chen, K. F. Karlsson, J. Birch and P. O. Holtz, *Sci. Rep.*, 2016, **6**, 21482.
47 D. Cherns, S. J. Henley and F. A. Ponce, *Appl. Phys. Lett.*, 2001, **78**, 2691–2693.

This journal is © The Royal Society of Chemistry 2018

48 W. Chen, T. Xu, F. He, W. Wang, C. Wang, J. Strzalka, Y. Liu, J. Wen, D. J. Miller, J. Chen, O. K. Hong, O. L. Yu and S. B. Darling, *Nano Lett.*, 2011, **11**, 3707–3713.

49 V. I. Arkhipov, P. Heremans and H. Bässler, *Appl. Phys. Lett.*, 2003, **82**, 4605–4607.

50 V. Arkhipov, E. Emelianova and H. Bässler, *Phys. Rev. Lett.*, 1999, **82**, 1321–1324.

51 Y. Yi, V. Coropceanu and J. Brédas, *J. Am. Chem. Soc.*, 2009, **131**, 15777–15783.

52 T. Itoh, S. Yano, N. Katagiri, Y. Iwabuchi, C. Gourdon and A. I. Ekimov, *J. Lumin.*, 1994, **60–61**, 396–399.

53 O. Rubel, S. D. Baranovskii, W. Stolz and F. Gebhard, *Phys. Rev. Lett.*, 2008, **100**, 1–4.

54 S. D. Baranovskii, M. Wiemer, A. V. Nenashev, F. Jansson and F. Gebhard, *J. Phys. Chem. Lett.*, 2012, **3**, 1214–1221.

55 G. Xing, N. Mathews, S. S. Lim, N. Yantara, X. Liu, D. Sabba, M. Grätzel, S. Mhaisalkar and T. C. Sum, *Nat. Mater.*, 2014, **13**, 476–480.

Published on 12 February 2018. Downloaded by Freie Universitaet Berlin on 2/14/2020 9:41:55 AM.